Exp. Theo. NANOTECHNOLOGY 10 (2026) 397-411 https://doi.org/10.56053/10.S.397

Well-modification pathway of hybrid structures by multi-wall carbon nanotube

Samah G. Ali[*], *Alwan M. Alwan, Allaa A. Jabbar*

Department of Applied Sciences, University of Technology, Baghdad-Iraq
[*]) Email: samahghanim97@gmail.com

Received 17/11/2025, *Received in revised form* 15/12/2025, *Accepted* 28/12/2025, *Published* 15/2/2026

In this paper, a novel approach in modifying the properties of hybrid structure of silver nanoparticle (AgNPs)/porous silicon (PSi) is carried out through deposition of multi wall carbon nanotubes (MWCNT); on PSi surface. The PSi layer is prepared by Photo-electrochemical etching technique using different current densities (15, 20, 25 and 30 mA/cm^2). The AgNPs/ MWCNT is deposited on the PSi surface by a simple ion reduction process using aqueous solutions of silver salt ($AgNO_3$) at 5×10^{-2} M, 10^{-2} M, 10^{-3} M, and 10^{-4} M concentrations. Structural, morphological and optical characterizations of (AgNPs/MWCNT/PSi) hybrid structures are analyzed in respect to the PSi layer morphology. The obtained results showed strong possibility of effectively controlling the morphological and structural properties of hybrid structure by controlling the pores' diameters. The deposition of the MWCNT and AgNPs on the walls and pores of the PSi structure enhanced the surface morphology of hybrid structure in addition to its specific surface area (S.S.A). The incorporating of MWCNT on the PSi substrate produced at 25 mA/cm^2 current density and 5×10^{-2} M $AgNO_3$ concentration led to higher specific surface area (S.S.A).

Keywords: Porous silicon, Etching technique, MWCNT, AgNPs, hybrid structure.

1. INTRODUCTION

Porous Silicon attracts much interest as a promising silicon-based nanostructure material for its unique properties [1]. It has been a desired material in many applications, particularly those involving chemical and biological sensing, where contact between the surface and the targeted molecules has been made possible due to the sponge structure and the vast internal surface area [2-3]. PSi is affordable, simple to produce, has the potential to infiltrate specific areas and can achieve high absorption coefficient and good sensing properties [4-7]. Porosity, size, and shape of pores strongly influence the PSi properties. The electrical and optical characteristics of silicon are thought to be effectively controlled by porosity. Etching settings can be utilized to adjust these characteristics [8-11]. Silver nanoparticles are the most

extensively studied metallic nanoparticles, because of their high possibility of connecting with numerous molecules or groups. Besides, they are simple to manufacture and functionalize. The plasmonic sensors of hybrid structure AgNPs/PSi have many applications in the chemical detection process. In addition, CNTs display high surface areas as fundamental qualities. They are highly desirable as substrates for heterogeneous catalysis due to their high electrical conducti vities, intrinsic size, and hollow architecture [12-17]. AgNPs/MWCNT has additional opportunities to use in electrochemical sensors; due to the electro-catalytic capabilities and significant increase of electron transfer rate [18-20]. One of the biggest challenges is managing the nanoparticle's size and its dispersion on a surface because of their tuned morphology and response traits [21-23]. MWCNTs and metal nanoparticles (AgNPs) hybrid materials have received a great deal of attention due to their peculiar electrical, chemical, and optical characteristics that depend on their size. Applications of MWCNT hybrid materials are found in several fields [24-27]. Generally, two methods exist for decorating carbon nanotubes with silver nanoparticles [28-30]. One is the deposition using an ion reduction procedure, where silver ions are formed on the sidewalls of carbon nanotubes; exposing the nanotubes to the silver ions. The latter are then reduced by the sidewalls of the nanotubes [31-35]. Increasing the surface area of plasmonic sensors made from hybrid nanostructures, porous silicon deposited with metal nanoparticles, is considered one of the most promising options to improve the performance of these sensors. These structures mainly work on the phenomenon of enhancing the intensity of the Raman signal scattered from the surface of the hybrid structures. In this work, a new path-way is suggested as a simple synthesis process to improve the characteristics of the AgNPs/MWCNT/PSi hybrid structure by controlling the pores dimensions, the main goal of this research is to propose an effective modification to the AgNPs/PSi hybrid structure to improve its structural and morphological properties using diluted concentrations of MWCNTs.

2. EXPERIMENTAL WORK

2.1 Chemical materials

Hydrofluoric acid (HF) 48% (CDH), India and Ethanol (C_2H_5OH) with purity of 99.9% (Sigma Aldrich), Germany are employed in etching process. Multi wall Carbon nanotubes (MWCNTs) with a diameter of 20-40nm, silver nitrate ($AgNO_3$) with purity of 95%, and sodium citrate ($Na_3C_6H_5O_7$) with purity of 99% are obtained from (Sigma Aldrich), Germany. The appropriate solution concentration is determined using equation (1).

$$\text{Molarity} = \frac{\frac{W}{M.wt}}{V} \quad (1)$$

where W represents the $AgNO_3$ and $Na_3C_6H_5O_7$ weight in (g), and M. wt refer to $AgNO_3$ and $Na_3C_6H_5O_7$ molarity weights which are about 107.8682 g/mol and 258.07 g/mol respectively. V Refer to the dissolved solution volume in (ml).

2.2 Formation of PSi

The PSi layer is formed using the photo-electrochemical etching (PEE) technique [36-39]. The etching cell consisted of two identical Teflon cylinders; the upper one contained a cylindrical cavity housing the etching solution, while the lower one is a solid shaft. The silicon wafer is placed on an aluminum foil and this combination is placed on the lower roller. The cavity between the two rollers is filled with the etching electrolyte solution. Etching is conducted either by applying a suitable current from a current source or by applying a voltage from a voltage supply. The positive electrode of the cell is the silicon while the negative electrode is platinum. The cell is filled with a (1:1) mixture of HF acid and ethanol. The photo-electrochemical etching set-up, shown in Figure (1), is performed at different current densities of (15, 20, 25 and 30) mA/cm^2 for 20 minutes, under a CW radiation from 635 nm and 150 mW/cm^2 laser diode.

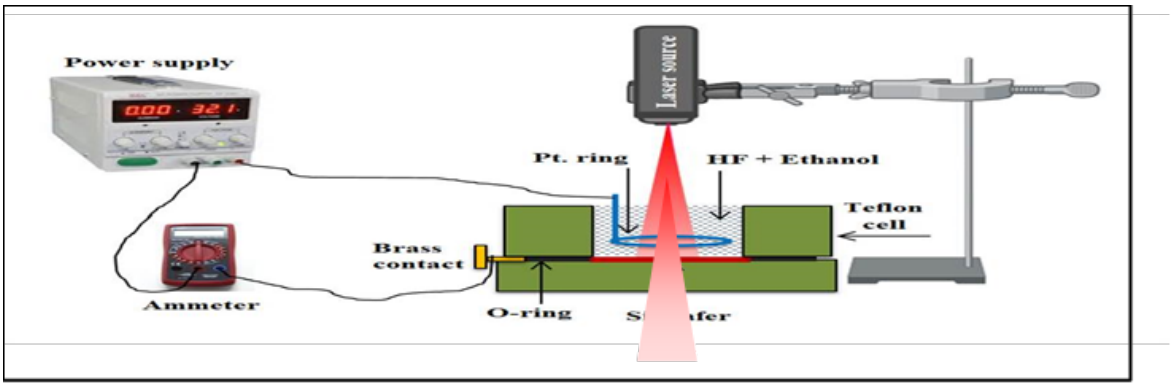

Figure 1 Schematic diagram of photo-electrochemical etching system.

2.3. Formation of AgNPs/PSi hybrid structure with and without MWCNT

Four milliliters (4 ml) of distilled water are mixed with silver salt at different concentrations, forming a solution of $AgNO_3$ silver salt that is deposited on the prepared porous silicon by drop casting, as shown in Figure (2a). To synthesis MWCNT suspension solution, 1.5 mg of carbon nanotubes is mixed with 4 ml of sodium citrate (suitable for depositing silver nanoparticles). The mixture is subjected to ultrasound for 15 minutes, then 100 ml of distilled water is added and the mixture is heated to the boiling point. Next, 4 ml of silver solution is added to the mixture and boiled for five minutes with continuous stirring. This is followed by magnetic stirring for half an hour to form silver nanoparticles deposited on carbon nanotubes. The schematic representation of forming the (AgNPs/MWCNT/PSi) hybrid structure is shown in Figure (2b). Carbons nanotubes decorated by silver nanoparticles are deposited on porous silicon by drop casting. The analysis of the FE-SEM images involving the surface density of pore, pore diameter and the particles size are computed using special software Image j8. Ag ions are reduced through the reaction below.

$$Ag^{+1} + e^{-} \rightarrow Ag \quad (2)$$

$$Si + 6HF \rightarrow H_2SiF_6 + 4H^{+} + 4e \quad (3)$$

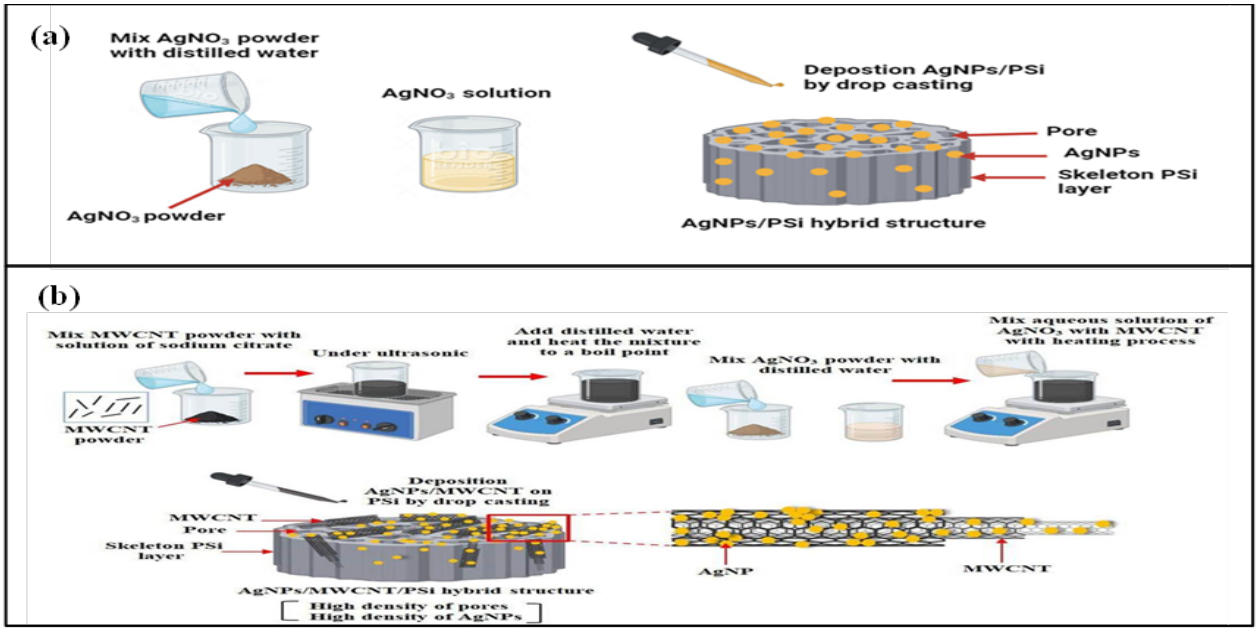

Figure 2 The schematic representation of formation (AgNPs/PSi) hybrid structure a) without MWCNT, b) with MWCNT.

3. RESULTS AND DISCUSSION

3.1 Morphological properties of formed Psi layer

The structural features of bare PSi layers such as the pore shape, their dimensions and wall sizes between neighboring pores depend intensively the applied current density. The morphological traits on the surface of PSi are investigated employing SEM (Scanning Electron Microscopy). Figure 3(a,d) displays the relevant surface shapes of the PSi structure formed at different current density values (15, 20, 25 and 30) mA/cm^2. At a low current density of etching of (15 mA/cm^2), Figure (3a) shows incomplete and asymmetric structure originated from overlapping pores between the individual pores and the arbitrary spread of these pores on the surface. Higher current density values have improved the etching route. The basic PSi layer appears as a pore-like cylindrical with a random distribution of pores. The rise in pore size has also led to an overlapping of the pores which disfigured their shapes. The accumulation of (e-h) pairs within the porous layer may be responsible for the pore diameters. By increasing the etching current density, the pore diameters increased. It ranged between (350-1100 nm) at a current density of (15 mA/cm^2) with (30 %) distribution of 550 nm. While and the pore sizes ranged between (950-3700 nm) at a current density of (30 mA/cm^2) with the highest distribution of (32%) at 2200 nm. The material's porosity layer after etching is calculated gravimetrically using equation (4) [40]. The values of the porosity are about 40%, 52%, 75% and 81% for etching current densities of 15, 20, 25 and 30mA/cm^2, respectively. The variations in the surface's pore sizes of the PSi layer could have resulted from the laser's Gaussian dispersion of light which may create asymmetric etching at the surface.

$$P(\%) = \frac{m1-m2}{m1-m3} \quad (4)$$

where Fresh silicon weights ml, m2 is the etched silicon weight, m3 is silicon weight after removing the PSi layer with 1 M of NaOH for 10 minutes, according to the formula. The porosity P(%) is a crucial factor in presenting the numbers of the formed pores on the PSi surface. Using equation (5), it is possible to calculate the PSi layer thickness as well.

$$d = \frac{m1-m3}{A \times W} \quad (5)$$

where d is the layer thickness, A is the silicon wafer's etched surface area, and W is the silicon density. In addition, the increase of the current density led to variation in the surface pores density within the porous matrix. The density of the pores, which represent the number of pores per unit area, are about (1.5×10^7, 1×10^8, 6×10^8, and 9×10^9 pores/cm^2) at current densities of (15, 20, 25 and 30 mA/cm^2), respectively. This surface density can be considered as a nucleation and growth sites for reduction of Ag^{+1} to Ag nanoparticles ($Ag^{+1} + e^- \rightarrow Ag$) and hence the development of the MWCNT on the porous structure. As the pores density increased the density of silver reduction sites (Si-H_x) bonds increased [41-43]. This led to an increase in the density of the AgNPs, which acts as a plasmonic active element to improve the SERS intensity.

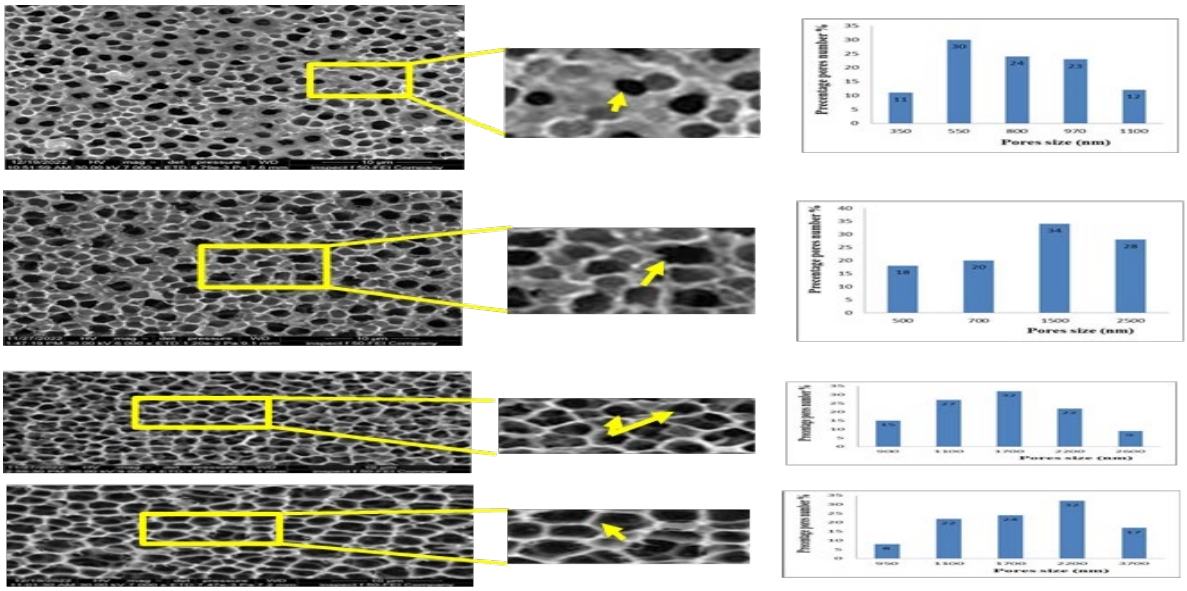

Figure 3 The SEM image of bare macro-PSi and statistical distribution of pore diameter as a function of current density (a) 15, (b) 20, (c) 25, and (d) 30 mA/cm^2.

3.2. Porosity and layer thickness

Porosity, layer thickness, and pore diameter are crucial criteria employed in examining the architectural properties of PSi. These properties depend on the etching circumstances, including etching current density, etching time and luminosity characteristics of the used laser. Figure (4a) demonstrates the reliance of the porosity on the etching current density. The porosity values increased from 40% for samples etched under (15mA/cm^2) to 81% for PSi etched under (30mA/cm^2). This behavior could be attributed to the increase of photo-induced holes within the porous structure. Thus improving the dissolution process of Si in the illuminated region ultimately increases the number and width of pores. Figure (4b) shows the thickness of the layer where the least significant value of (3.8 μm) is at (15 mA/cm^2) and the greatest value is (8.6 μm) at (30 mA/cm^2). It is clear that the association between the layer thickness and the etching current density is quasilinear. The interpretation of this behavior is that the dissolution process of Si occurs within the pore layer itself instead of other areas. Porosity and layer thickness are calculated using equations 4 and 5, respectively. As for Figure (4c), the pore diameter increases linearly to reach (2200 nm) at a current density of (30 mA/cm^2).

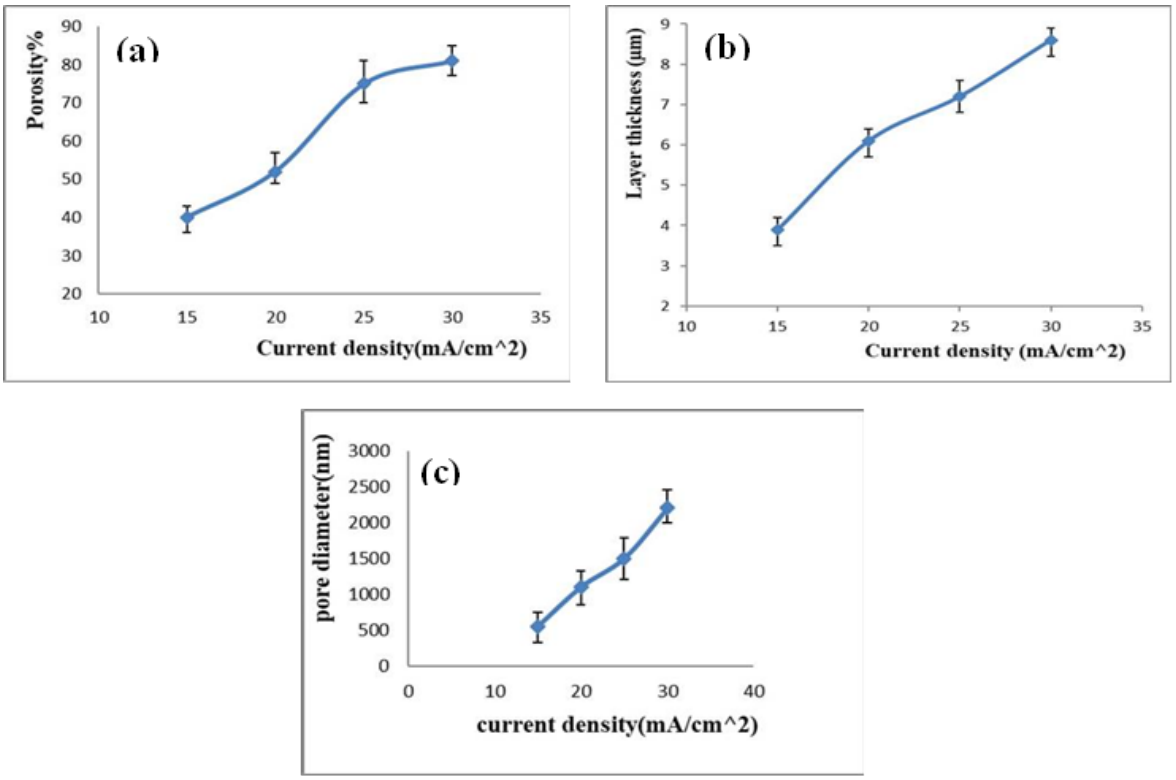

Figure 4 (a) Porosity (b) layer thickness and (c) pore diameter with current density.

3.3 Morphological properties of hybrid structure before incorporated MWCNT

The growth of AgNPs nanoparticles is dependent on the formation of dangling bond groups. When a fixed surface morphology of the formed PSi layer has been used, the variation in the deposited AgNPs layer modifies the structural properties of the PSi surface due to its dependence on the nanoparticle's density and distribution. Figure (5) shows an SEM image of silver nanoparticles drop casted on PSi without applying an external voltage. The shape of the deposited AgNPs at each concentration had a uniform distribution as the PSi layer possessed an almost uniform distribution of pore sizes with low surface roughness. Silver regions tend to form large continuous areas on the surface resembling plating process. Thus, the amount of AgNPs regions can be predicted to develop outside the pore itself. This could be explained by the formation dependence of the AgNPs on ($Si-H_x$) dangling bond groups. It is been reported that the deposition of metal nanoparticles with a certain concentration volume is harder due to the random distribution of ($Si-H_x$) dangling bonds and groups on the porous surface, as well as the uncontrolled movement of silver [44]. Figure (5) illustrates that as the concentration of $AgNO_3$ decreases, the density of silver nanoparticles decreases.

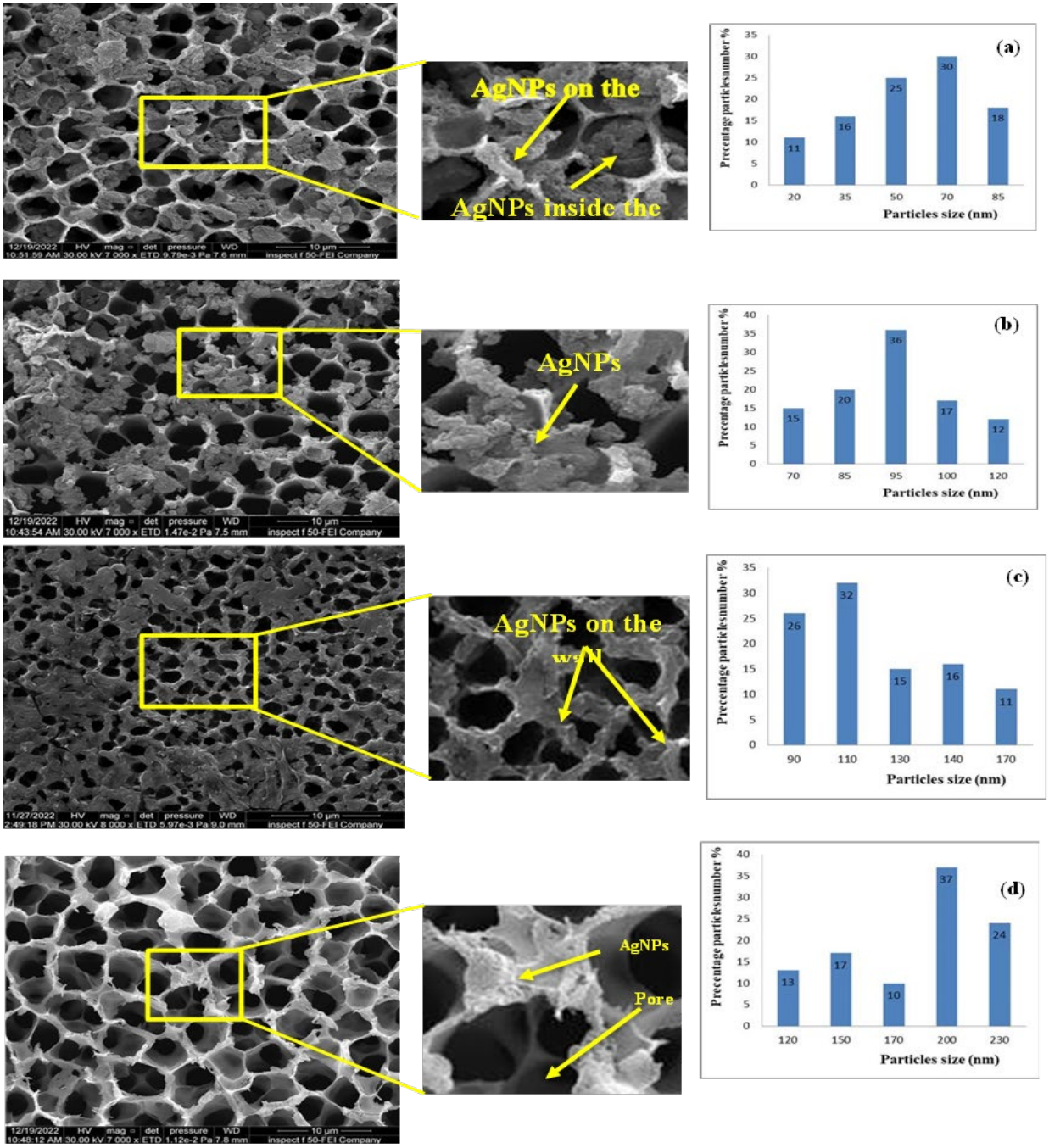

Figure 5 The SEM image of AgNPs/PSi hybrid structure and their statistical particle distributions over PSi after deposition for a different AgNPs concentration. (a) 5×10^{-2}M, (b) 10^{-2}M, (c) 10^{-3}M, (d) 10^{-4}M.

The same PSi surface morphology has been used to investigate the dependence of AgNPs deposition on PSi using different concentrations of (5×10^{-2}, 10^{-2}, 10^{-3} and 10^{-4} M) under 20 min etching time and etching current density of 25 mA/cm^2. Reducing the concentration of the $AgNO_3$ solution on the PSi layer reduces the rate of ion reduction and thus the density of the deposited silver nanoparticles. Thus, porous substrate is transformed from almost completely covered with AgNPs at high concentrations of (5×10^{-2} and 10^{-2} M) as shown in Figure 5(a,b) to partially covered with AgNPs at low concentrations (10^{-3} and 10^{-4} M) as shown in Figure 5 (c,d). The process of AgNPs reduction by dangling bonds of the porous layer is given by equations (2). The statistical distribution is a function of the deposition of silver

nanoparticles at different concentrations. As shown in Figure (5a), when the silver concentration is 5×10^{-2} M, the distribution ranged from (20-85) nm with the highest distribution value 70 nm (30%), as in Figure (5d), the silver concentration is 10^{-4} M and the distribution ranged from (120- 230) nm, with the highest distribution value 200 nm (37%).

3.4. With incorporated MWCNT

Figure 6 displays the effect of changing the concentration of silver nanoparticles (5×10^{-2}, 10^{-2}, 10^{-3} and 10^{-4}) M on the morphology of the synthesized hybrid structure prepared at the etching current density (25mA/cm²) with incorporated MWCNT.

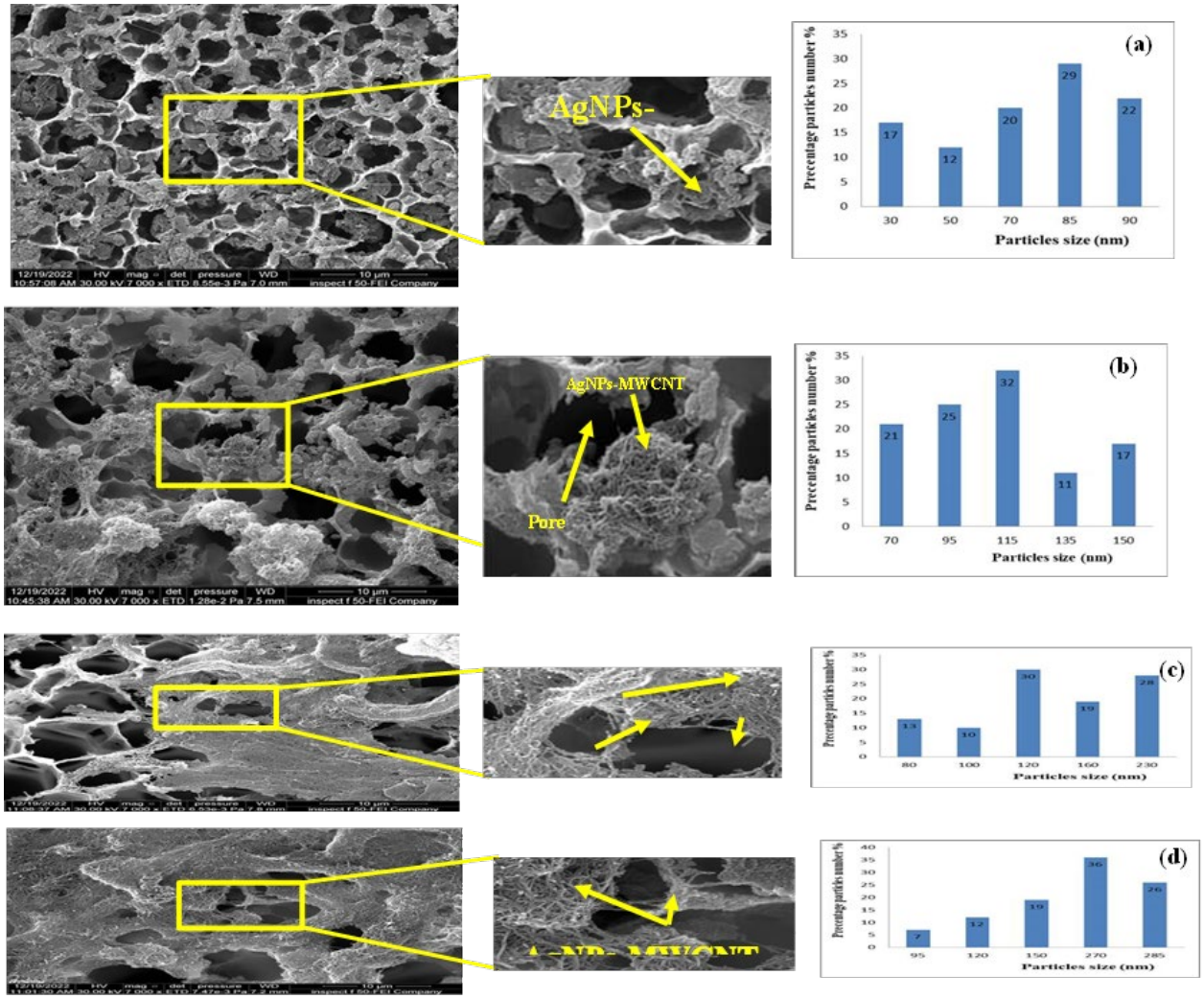

Figure 6 The SEM image of AgNPs/MWCNT/PSi hybrid structure and their statistical particle distributions over PSi after deposition for a different AgNPs concentration with incorporated. a) 5×10^{-2}M, b) 10^{-2}M, c) 10^{-3}M, d) 10^{-4}M.

The effect of silver nanoparticles concentration variation on the morphology of the resulted surface with fixing both the pore morphologies and the carbon nanotubes concentration is studied, see Figure 6(a,d). It is clear that the increase in the concentration of silver ions led to an increase in the growth rate of silver nanoparticles, placed on the carbon nanotubes. This improved the specific surface area (S.S.A) of the integrated porous, carbon nanotube with the AgNPs to a large extent leading to enhance the sensing process effectively. Also, the MWCNT improved the surface density of AgNPs, which undecorated the MWCNT, to (8×10^{9}, 3×10^{9}, 8×10^{8}, 5×10^{8} AgNPs/cm²). The analyses of the FE-SEM image, involving

the surface density of (AgNPs) particle size are computed by Image j8 software. The study confirmed the presence of AgNPs/MWCNT on the PSi surface and showed the statistical distribution of nanoparticle sizes for four samples prepared under different $AgNO_3$ concentrations. It can be clearly seen the random distribution of AgNPs on the porous and MWCNT layers. The resulted size distribution of AgNPs increased with the decrease of $AgNO_3$ concentration. This is confirmed by the statistical distribution, as the particle size of the AgNPs ranged from (30-90) nm and the peak size is about 85 nm, 29% when the silver concentration is (5×10^{-2} M). While, the size of the AgNPs ranged from (95-285) nm and the peak size is about 270 nm, grow by 36% when the silver concentration is (10^{-4} M). The minimum size distribution of AgNPs obtained at $AgNO_3$ concentration of 5×10^{-2} M. this ensured the surface area high value, thus this $AgNO_3$ concentration is endorsed.

3.5. Optical properties of formed PSi layer, hybrid structure Agnps/PSi with and without MWCNT

The PL spectra of porous silicon samples before and after the deposition process are conducted. Figure 7 shows the black curve the PL spectrum of a porous silicon sample prepared at an etching current density of 25 mA/cm^2 for 20 min. PL spectrum is measured by exciting the PSi samples using a wavelength of (325 nm). Figure 7 shows the red curve the PL extracted from porous silicon samples deposited with silver nanoparticles AgNPs/PSi at a concentration of (5×10^{-2} M) and a current density of 25 mA/cm^2. This increase in PL intensity is is introduced by a shift occurs due to quantum confinement effects in the hybrid structure AgNPs/PSi due to the presence of the silver nanoparticles leading to high PL peaks. The photoluminescence intensity and peaks location provide comprehensive information about the surface nature of the hybrid structure AgNPs/PSi. This information depends on the sizes of the aggregated AgNPs, their positions on the PSi surface. The deposition of AgNPs affects the PSi and its surface contents, which has the effect of either enhancing or suppressing the PL intensity. As for Figure 7 the blue curve the AgNPs/MWCNT/PSi hybrid structure showed greater PL intensity compared to both PSi and AgNPs/PSi samples. The presence of (MWCNT) decorated with silver nanoparticles (AgNPs) led to the suppression of dangling bonds. These bonds act as non-radioactive contact points for recombination. Extinguishment among these sites is used to improve the intensity of PL. In addition, adding carbon nanotubes to AgNPs/PSi hybrid composite led to surface enhancement and improved the structural properties of the AgNPs/PSi hybrid structure. The ratio between the PL intensity of PSi nanoparticles treated with silver nanoparticles and the PL intensity of the particles before and after the modification had an improvement factor of (1.7 and 2.9) as shown in Table (1). Utilizing the subsequent formula, the PSi volume value is determined by equation (6) [45].

$$E_{g_{psi}} = E_{g_{si}} + \frac{88.34}{L^{(1.37)}} \quad (6)$$

where E_{gPSi} (eV) is the energy bandgap of porous silicon (eV) is calculated according to the following equation ($E_{g_{psi}} = \frac{hc}{\lambda}$), E_{gSi} is the energy bandgap of bulk silicon (1.12 eV), and L is the porous silicon size in (nm).

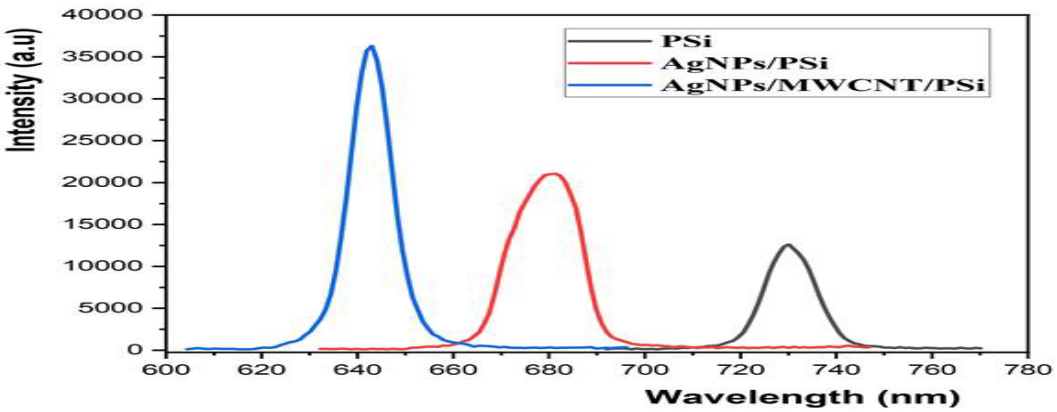

Figure 7 Photoluminescence spectra of bare-PSi, AgNPs/PSi, and AgNPs/MWCNT/PSi hybrid structure.

Table 1 The photoluminescence calculations of bare PSi, AgNPs/PSi with and without MWCNT**.**

Hybrid structure	Wavelength (nm)	Energy gap (eV)	Si Nano Crystalline (nm)	Intensity (a.u)	Improvement Factor = (intensity after/intensity before)
Bare PSi	730	1.698	4.045	12620	—
AgNPs/PSi	680	1.823	3.378	20986	1.7
AgNPs/MWCNT/PSi	644	1.925	3.057	36297	2.9

3.6. EDX and X-ray diffraction analysis of hybrid structures

Figure 8 shows nanoparticle components made of $AgNO_3$, MWCNT deposited on a PSi substrate, proving the formation success of AgNPs and AgNPs-MWCNT. It is observed that when nano-materials are deposited on the PSi substrate, the porous silicon element began to decrease, which confirmed that PSi is partially covered by the deposited nano materials. While, the presence of oxygen is associated with the presence of an original oxide layer on top of the hybrid structure.

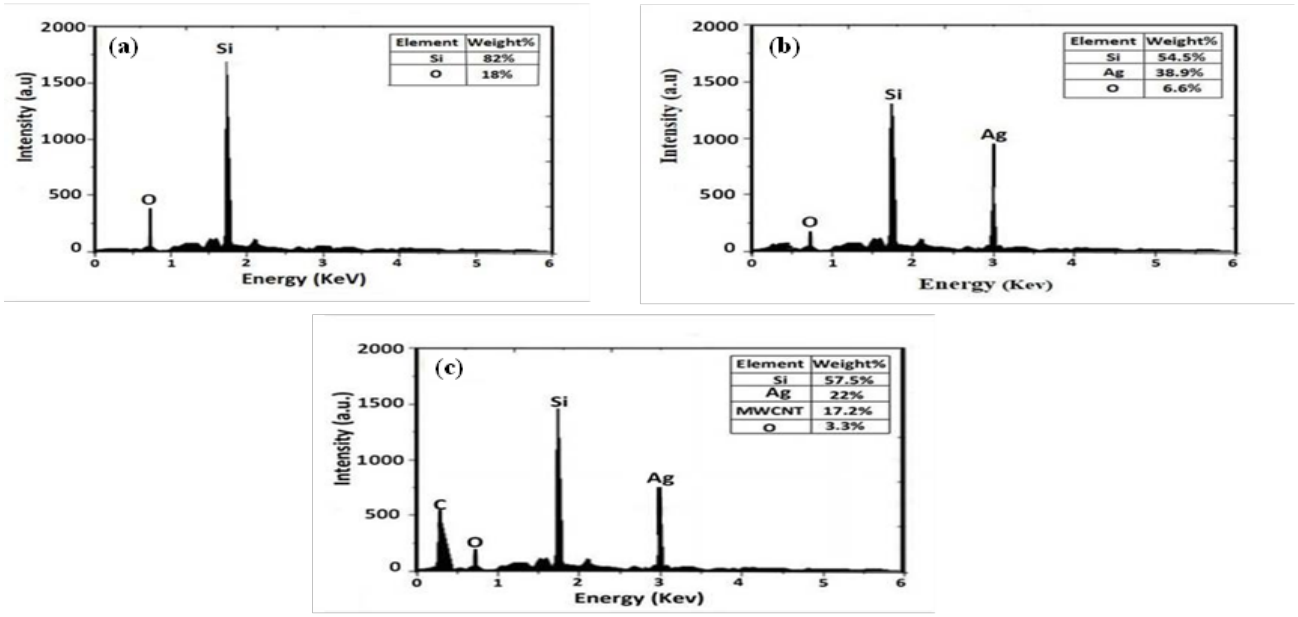

Figure 8 Illustrates the EDX pattern for a) bare PSi b) AgNPs/PSi hybrid structure c) AgNPs/MWCNT/PSi hybrid structure.

The XRD of PSi (prepared at 25 mA/cm^2 current density), the AgNPs/PSi hybrid structure (prepared from 5×10^{-2} M AgNPs concentration) and the AgNPs/MWCNT/PSi hybrid structure are shown in Figure (9). Figure (9a) represents the XRD of PSi at 2Θ° of about (33.5). While in Figure (9b), the XRD spectrum shows the existence of individual peaks related to AgNPs. XRD is an effective equipment for nanoparticle structure detection, especially for hybrid structures. Broad and defined peaks are detected at 2Θ° [46-47].

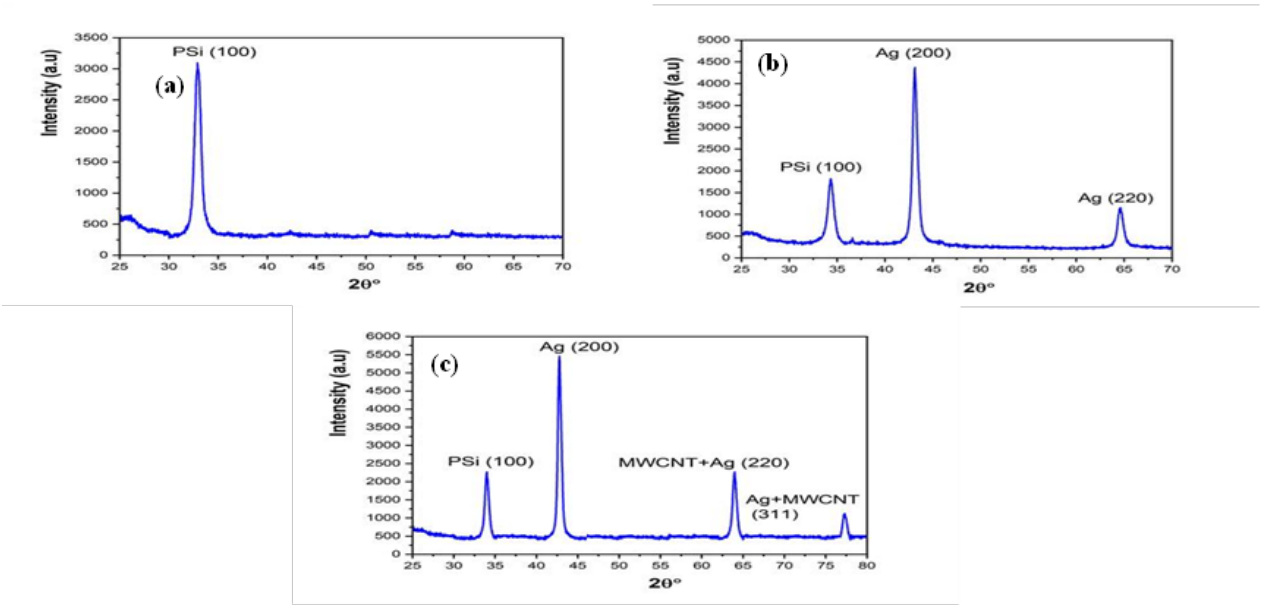

Figure 9 The X-ray diffraction analysis for a) bare PSi b) AgNPs/PSi hybrid structure c) AgNPs/MWCNT/PSi hybrid structure.

In addition, Figure (9c) illustrates the existence of a peak resulted from overlapping the individual XRD peaks of AgNPs and MWCNT at plane (220) and plane (311). This peak has a broadened FWHM which means different nanoparticle sizes and S.S.A. All diffraction values are applied to calibrate the diffraction card in Figure 9(a-c). The values of Nano-silicon appear with a diffraction angle of 33.5 in the (100) plane. The XRD pattern of the hybrid structure shows the diffraction peaks at 44, 64.8, 64.3 and 77.2 which can be related to (200), (220), and (311) planes [48]. This outcome is reasonably consistent with the results presented in the data JCPDS card 96-101-1061 for (PSi), JCPDS-ICDD card no.04-802 for (MWCNT) and JCPDS card 27-1402 for (AgNPs). Two peaks at 64.3 and 77.2 are found coincidentally between the Ag peaks and the MWCNT peaks. The width of the diffraction peak is affected by the sizes and the quantity of the nanomaterials. The XRD analysis shows the presence of porous silicon, carbon nanotubes and silver nanoparticles. From the figure, it can be seen that the porous silicon peaks are still present and visible at the plane (100), but when the AgNPs/PSi hybrid composite is present with and without MWCNT, the peaks of the porous silicon peak began to decreases [49] [50]. The XRD peaks are calculated applying Scherer's equation.

$$L = \frac{0.9\lambda}{\beta COS\theta} \tag{7}$$

where (L) is the grain size for Ag, MWCNT, and Ag-MWCNT in (nm), (λ) is the applied radiation's wavelength, expressed in nanometers (nm), (β) is the Full width at half maximum (FWHM) is expressed in (radians), (Θ) is the diffraction angle is expressed in (radians), and the shape factor value is 0.9 [50-51].

One of the merits of the nanostructure material is its specific surface area (S.S.A.), which is expressed as in equation (8);

$$S.S.A = \frac{6000}{L*\rho} \tag{8}$$

where D is the density of silver nanoparticles and multi wall carbon nanotubes (approximately 10.5 and 1.7 g/cm^3) [51]. However, the density of Ag-MWCNT is 9.62 g/cm^3, which could be determined using equation (9) which depends on the findings of an EDS [52].

$$D = \frac{a*\rho 1+b*\rho 2}{a+b} \tag{9}$$

where, D= density of Ag-MWCNT alloy nanoparticles, g/m^3; a=wt. % Ag and b=wt. % MWCNT, the AgNPs, MWCNT and alloy AgNPs/MWCNT size and (S.S.A.) are developed in Table (2).

Table 2 Particles sizes, specific surface area with and without MWCNT for hybrid structure.

Hybrid structure	Phase	2θ°	FWHM	L(nm)	S.S.A(m^2/gm)
AgNPs/PSi	200	44	0.63332	13.53	42.24
	220	64.8	0.75754	12.42	46.01
AgNPs/MWCNT/PSi	220	64.3	0.78868	11.89	52.42
	311	77.2	0.99167	10.27	60.73

4. CONCLUSIONS

In this work, a novel approach in modifying the structural properties of AgNPs/MWCNT/PSi was satisfied by a simple, low cost and easy-run ion reduction process of PSi in an aqueous solution of $AgNO_3$ and MWCNT. That the results show clearly that the process of modifying the properties of a hybrid structure depends on the porosity of the PSi layer and the concentration of silver ions. The surface area increases significantly when MWCNT is deposited on the boundaries of the pores instead of when the deposition is inside the pores. Finally, the morphological properties of the resulting hybrid structure depend on the porous layer.

ACKNOWLEDGMENTS

The authors express gratitude to their respective universities for providing encouragement and infrastructure.

Declaration of interests:

The authors declare that they have no known competing financial interests or personal relationships that could have appeared to influence the work reported in this paper.

Data availability

All data included in this paper are available upon request by contact with the contact corresponding author.

Funding

The authors declare that no funds, grants, or other support were received during the preparation of this manuscript.

Author Contribution

Prof. Dr. Alwan Mohammed Alwan prepared figures. Dr. Allaa A.Jabbar devised the idea and helped while preparing and supervising the final draft. Samah G. Ali wrote the main manuscript text. All authors reviewed the manuscript.

Ethical Approval

Not applicable.

References

[1] A. K. Rahman, L. S. Chen, M. I. Al-Khalidi, Exp. Theo. NANOTECHNOLOGY 10 (2026) 115–124 https://doi.org/10.1234/etnano.2026.115
[2] A.A. Khalaf, A.H. Attallah, A.B. Dheyab, A.M. Alwan, J. Phys.: Conf. Ser. 1963 (2021) 0120xx https://doi.org/10.1088/1742-6596/1963/1/0120xx
[3] L.A. Golovan, V.Yu. Timoshenko, J. Nanoelectron. Optoelectron. 8 (2013) 223–239 https://doi.org/10.1166/jno.2013.1474
[4] S.S. Khudiar, U.M. Nayef, F.A. Mutlak, J. Nanosci. Nanotechnol. 2 (2022) 64–69
[5] A.M. Alwan, Eng. Technol. J. 25 (2007) 1143–1148
[6] A.Yu. Panarin, S.N. Terekhov, K.I. Kholostov, V.P. Bondarenko, Appl. Surf. Sci. 256 (2010) 6969–6976 https://doi.org/10.1016/j.apsusc.2010.04.101
[7] Z.J. Abdul Kareem, U.M. Nayef, K.A. Hubeatir, Eng. Technol. J. 33 (2015) 595–601
[8] M.V. Chursanova, L.P. Germash, V.O. Yukhymchuk, V.M. Dzhagan, I.A. Khodasevich, Appl. Surf. Sci. 256 (2010) 3369–3373 https://doi.org/10.1016/j.apsusc.2009.12.017
[9] M. Alwan, O.A. Abdulrazaq, Int. J. Mod. Phys. 22 (2008) 417–422
[10] N.S. Dawood, M.Q. Zayer, M.F. Jawad, Karbala Int. J. Mod. Sci. 8 (2022) Article 11 https://doi.org/10.1016/j.kijoms.2022.11.001
[11] K.A. Wepasnick, B.A. Smith, J.L. Bitter, Anal. Bioanal. Chem. 396 (2010) 1003–1014 https://doi.org/10.1007/s00216-009-3286-8

[12] S. Shahrokhian, S. Rastgar, Electrochim. Acta 78 (2012) 422–429 https://doi.org/10.1016/j.electacta.2012.06.019
[13] M.Q. Zayer, M. Alwan, A.S. Ahmed, A.B. Dheyab, Curr. Appl. Phys. 19 (2019) 1024–1030 https://doi.org/10.1016/j.cap.2019.06.007
[14] G.A. Rance, D.H. Marsh, S.J. Bourne, ACS Nano 4 (2010) 4920–4928 https://doi.org/10.1021/nn100897r
[15] D. Eder, Chem. Rev. 110 (2010) 1348–1385 https://doi.org/10.1021/cr800433k
[16] D.H. Marsh, G.A. Rance, R.J. Whitby, J. Mater. Chem. 18 (2008) 2249–2256 https://doi.org/10.1039/B718217D
[17] H. Ozawa, X. Yi, T. Fujigaya, Y. Niidome, T. Asano, N. Nakashima, J. Am. Chem. Soc. 133 (2011) 14771–14777 https://doi.org/10.1021/ja204433d
[18] R. Das, S. Upadhyay, M.K. Sharma, RSC Adv. 5 (2015) 48147–48153 https://doi.org/10.1039/C5RA05210A
[19] G.G. Wildgoose, C.E. Banks, R.G. Compton, Small 2 (2006) 182–193 https://doi.org/10.1002/smll.200500334
[20] P. Yanez-Sedeno, J.M. Pingarron, J. Riu, Trends Anal. Chem. 29 (2010) 939–953 https://doi.org/10.1016/j.trac.2010.05.002
[21] J. Wang, Electroanalysis 17 (2005) 7–14 https://doi.org/10.1002/elan.200403113
[22] D. Vairavapandian, P. Vichchulada, M.D. Lay, Anal. Chim. Acta 626 (2008) 119–129 https://doi.org/10.1016/j.aca.2008.07.015
[23] M. Ghalkhani, S. Shahrokhian, F. Ghorbani-Bidkorbeh, Talanta 80 (2009) 31–38 https://doi.org/10.1016/j.talanta.2009.06.048
[24] M.A. Herrero, J. Guerra, V.S. Myers, M.V. Gomez, R.M. Crooks, ACS Nano 4 (2010) 905–912 https://doi.org/10.1021/nn901830u
[25] Y. Guo, S.H. Guo, Y. Fang, S.H. Dong, Electrochim. Acta 55 (2010) 3927–3931 https://doi.org/10.1016/j.electacta.2010.02.016
[26] M.P.N. Bui, X.H. Pham, K.N. Han, Electrochem. Commun. 12 (2010) 250–253 https://doi.org/10.1016/j.elecom.2009.11.039
[27] B.K. Jena, C.R. Raj, Anal. Chem. 78 (2006) 6332–6339 https://doi.org/10.1021/ac060686r
[28] R. Zanella, E.V. Basiuk, P. Santiago, J. Phys. Chem. B 109 (2005) 16290–16295 https://doi.org/10.1021/jp0522177
[29] L. Liu, T. Wang, J. Li, Chem. Phys. Lett. 367 (2003) 747–752 https://doi.org/10.1016/S0009-2614(02)01725-3
[30] R. Zhang, M. Hummelgard, H. Olin, Mater. Sci. Eng. B 158 (2009) 48–52 https://doi.org/10.1016/j.mseb.2008.12.015
[31] R.S. Singh, T. Premkumar, J.Y. Shin, K.E. Geckeler, Chem. Eur. J. 16 (2010) 1728–1743 https://doi.org/10.1002/chem.200901845
[32] A.V. Ellis, K. Vijayamohanan, R. Goswami, Nano Lett. 3 (2003) 279–282 https://doi.org/10.1021/nl025924f
[33] M.-C. Daniel, D. Astruc, Chem. Rev. 104 (2004) 293–346 https://doi.org/10.1021/cr030698
[34] P.F. Qi, O. Vermesh, M. Grecu, Nano Lett. 3 (2003) 347–351 https://doi.org/10.1021/nl034748j
[35] S.K. Abbas, A.N. Naje, Iraqi J. Phys. 18 (2020) 62–72
[36] S.K. Abbas, A.N. Naje, J. Nanoelectron. Phys. 11 (2015) 05015 https://doi.org/10.21272/jnep.11(5).05015
[37] V.E. Kan, V.V. Bolotov, K.E. Ivlev, Procedia Eng. 152 (2016) 706–710 https://doi.org/10.1016/j.proeng.2016.07.675
[38] M. Alwan, R.B. Rashid, A.B. Dheyab, Iraqi J. Sci. 59 (2018) 57–66
[39] L.A. Wali, K.K. Hasan, M. Alwan, Plasmonics 15 (2020) 985–993 https://doi.org/10.1007/s11468-019-01072-8
[40] A.A. Jabbar, M. Alwan, M.Q. Zayer, A.J. Bohan, Mater. Chem. Phys. 241 (2019) 122359 https://doi.org/10.1016/j.matchemphys.2019.122359

[41] M. Alwan, M.Q. Zayer, A.A. Jabbar, J. Theor. Appl. Phys. 14 (2020) 61–70 https://doi.org/10.1007/s40094-019-00364-0
[42] W.K. Hamoudi, M. Alwan, D.S. Jubair, AIP Conf. Proc. 2372 (2021) 080019 https://doi.org/10.1063/5.0066596
[43] A.G. Cullis, L.T. Canham, P.D.J. Calcott, J. Appl. Phys. 82 (1997) 909–965 https://doi.org/10.1063/1.366168
[44] D.A. Hashim, M. Alwan, M.F. Jawad, J. Electrochem. Soc. 165 (2018) 773–778 https://doi.org/10.1149/2.0221810jes
[45] H.R. Abed, M. Alwan, A.A. Yousif, Opt. Quantum Electron. 51 (2019) 333 https://doi.org/10.1007/s11082-019-2050-0
[46] M. Alwan, A.B. Dheyab, A.J. Allaa, Eng. Technol. J. 35 (2017) 811–815
[47] M. Alwan, A.A. Jabbar, Mod. Appl. Sci. 5 (2011) 106–112 https://doi.org/10.5539/mas.v5n6p106
[48] N.M. Ahmed, Y. Al-Douri, M. Alwan, Procedia Eng. 53 (2013) 393–399 https://doi.org/10.1016/j.proeng.2013.02.051
[49] M. Alwan, D.A. Hashim, M.F. Jawad, Solid State Electron. 153 (2019) 75–81 https://doi.org/10.1016/j.sse.2018.11.006
[50] H.S. Faisal, C.M. Ahmed, A.A.A. Mohammed, Exp. Theo. NANOTECHNOLOGY 9 (2025) 571–589 https://doi.org/10.1234/etnano.2025.571
[51] S.S. Ba Hashwan, M.H. Md Khir, I.M. Nawi, Exp. Theo. NANOTECHNOLOGY 9 (2025) 539–553 https://doi.org/10.1234/etnano.2025.539
[52] A.T. Al-Douri, A.A. Khaleel, L.M. Ibrahim, Exp. Theo. NANOTECHNOLOGY 9 (2025) 563–569 https://doi.org/10.1234/etnano.2025.563